Journal of Geochemical Exploration 182 (2017) 110–120

Contents lists available at ScienceDirect

Journal of Geochemical Exploration

journal homepage: www.elsevier.com/locate/gexplo

# Mineral chemistry and P-T conditions of the adakitic rocks from Torud–Ahmad Abad magmatic belt, S-SE Shahrood, NE Iran

Fazilat Yousefi[a,*], Mahmoud Sadeghian[a], Christina Wanhainen[b], Habibollah Ghasemi[a], Papadopoulou Lambrini[c], Glenn Bark[b], Mehdi Rezaei-Kahkhaei[a], Antonios Koroneos[c]

[a] Faculty of Earth Sciences, Shahrood University of Technology, Shahrood, Iran
[b] Department of Civil, Environmental and Natural Resources Engineering, Lulea University of Technology, Lulea, Sweden
[c] Department of Mineralogy-Petrology-Economic Geology, Aristotle University of Thessaloniki, Thessaloniki, Greece

ARTICLE INFO

*Keywords:*
Mineral chemistry
P-T
Crystallization
Adakite
Torud–Ahmad Abad Magmatic Belt

ABSTRACT

Torud-Ahmad Abad magmatic belt is located 175 km east and southeast of Shahrood in the northern part of the Central Iran Structural Zone and includes a thick sequence of Paleocene to middle Eocene volcanic and volcanosedimentary rocks. This magmatic belt was formed by numerous hypabyssal igneous adakitic domes constituting basaltic andesite, andesite, trachyandesite, dacite, trachydacite, and dacite. The investigated rocks are mainly composed of pyroxene, amphibole, and plagioclase, with minor biotite and opaque minerals. Mineral chemical analysis reveals that plagioclase composition varies from albite to labradorite, clinopyroxene varies from diopside to augite, and amphibole varies from Mg-hastingsite to Mg-hornblende.

Amphibole geothermobarometry suggests crystallization temperatures of 850–1050 °C, at 2–6 kbar and the temperature of 920–970 °C, at a pressure of 3–4.5 kbar, which are conditions in agreement with andesite and dacite formation. Clinopyroxene crystallized at temperatures of 1020–1170 °C, at 2–10 kbar, indicating crystallization at crustal depths of maximum 30 km for the studied intrusive rocks in the Torud-Ahmad Abad magmatic belt.

## 1. Introduction

The mineral assemblages and the composition of minerals in magmatic rocks are related to the composition and evolving conditions of the melt during crystallization (Abbott and Clarke, 1979; Helmy et al., 2004). This is the reason for using the composition of minerals in deciphering the physicochemical parameters of crystallization pressure and temperature (Helmy et al., 2004). Amphibole and clinopyroxene thermobarometry have been widely used to estimate the emplacement pressure (P) and temperature (T) of calc-alkaline igneous rocks, thereby providing a tool to determine the depth of emplacement of a rock (Anderson and Smith, 1995; Putirka, 2008b; Ridolfi et al., 2010; Jamshidi et al., 2015). The studied hypabyssal igneous rocks intruded into Eocene volcanic and volcanosedimentary rocks. They are composed of andesite, trachyandesite, basaltic trachyandesite, trachydacite and dacite (Yousefi et al., 2017). Major minerals include amphibole, pyroxene, and plagioclase. Amphibole and clinopyroxene also constitute the most common phenocrysts in these rocks, and have thus been used for estimating the pressure-temperature conditions, and the depth of final emplacement of the magma. Mineral zoning has also been investigated in this study. Zoning of minerals have received a great deal of attention since it records physical and chemical changes in the magmatic liquids from which the crystals grow (Blundy and Shimizu, 1991). This paper presents mineral chemistry obtained by scanning electron microscope analysis, from the andesitic and dacitic rocks of adakitic nature in the south and southeast of Shahrood in northeast Iran. We investigate the depth of magma chambers through geothermobarometric calculations based on the mineral compositions.

### 1.1. Geological setting

The studied adakitic rocks are located to the south and southeast of Shahrood city, in the northern part of the Central Iran Structural Zone (Fig. 1). Remnants of Cenozoic magmatic activity can be observed in most parts of Iran, except in the Zagros (west–southwest of Iran) and Kopeh Dagh (northeast of Iran) areas (Nabavi, 1976; Moeinvaziri, 1996; Darvishzadeh, 2004). During the Mesozoic and Cenozoic, the Central Iran Structural Zone was a tectonically dynamic region. In addition to several well-defined deformational events, magmatic activity can be traced in the form of volcanic and subvolcanic rocks, and intrusive

* Corresponding author.
*E-mail address:* f.yousefi87@gmail.com (F. Yousefi).

http://dx.doi.org/10.1016/j.gexplo.2017.09.006
Received 19 March 2017; Received in revised form 25 August 2017; Accepted 8 September 2017
Available online 18 September 2017
0375-6742/ 

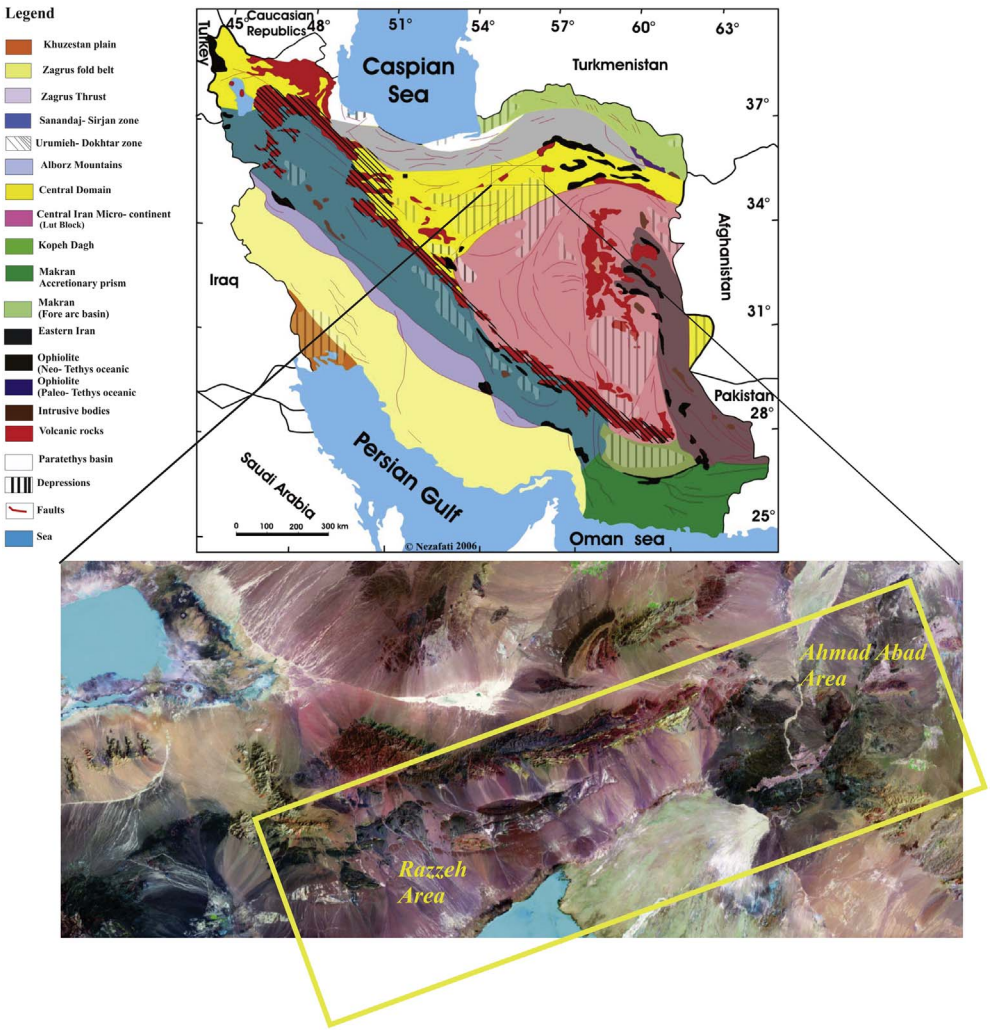


**Fig. 1.** The study area is shown by a rectangle in an image taken from Mrsid viewer pictures (geographic coordinates: 35° 34′ to 35° 43′ north latitude and 55° 11 to 56° 35′ eastern longitude) (Nezafati, 2015).

bodies, especially of Cenozoic age (Rahmati Ilkhchi, 2009). In this area, volcanic and volcanosedimentary rocks of Late Paleocene to Middle Eocene are intruded by numerous middle-late Eocene adakitic domes and dikes (Fig. 2). Towards the east, these adakitic rocks have intruded into the Sabzevar ophiolitic complex (Jamshidi et al., 2015). These domes and dikes crop out in an extensive area to the south and southeast of Shahrood, and are the subject of our detailed mineral chemistry investigation. Various types of enclaves of different sizes and shapes have been found in the mentioned rocks. These enclaves are evidences of magma mixing and crustal contamination. Petrology, geochemistry, and tectonic setting together with evidences for magma mixing and crustal contamination of these rocks have previously been studied by Yousefi et al. (2016, 2017). The geochemistry of the studied rocks, e.g. the enrichment in LREE and LILE and depletion in HREE and HSFE, as well as a silica content varying between 59 and 63 wt% and 5–59 wt%, a $Na_2O$ content of > 3 wt%, an $Al_2O_3$ content of > 16 wt%, an Yb content of < 1.8 ppm, and an Y content of < 18 ppm, indicate that they are adakite-like or adakitic rocks. The adakitic nature of these rocks has previously been documented by Yousefi et al. (2016, 2017), Jamali (2014) and Mansouri Moghaddam (2014). These rocks penetrate a thick volcanosedimentary sequence of Late Paleocene to middle Eocene age (Fig. 1) and are related to the subduction of the Neo-Tethyan oceanic slab of the Sabzevar–Darouneh branch beneath the continental crust of the northern part of the Central Iran Structural Zone (Ghasemi and Rezaei Kahkhaei, 2015 and Yousefi et al., 2016).

### 1.2. Analytical methods

After determining the composition of the rocks in the Torud-Ahmad Abad magmatic belt (see Yousefi et al., 2017 for details), twelve samples of dacitic and andesitic rocks were selected for analysis of mineral phases. Thin section preparation and polishing for mineralogical analysis was done in the Grona Geology Laboratory in Tehran, Iran. Mineral analysis was performed at Aristotle University of Thessaloniki and comprises 245 analyses of amphibole, 370 analyses of feldspars and 51 analyses of pyroxenes. Analyses were carried out in the Scanning Electron Microscope Laboratory, using a SEM (JEOL JSM-840A) equipped with an energy dispersive spectrometer (EDS, Oxford INCA 250). The analytical setting was 20 kV accelerating voltage with a 0.4 mA probe current. A pure Co standard was used for calibrating the EDS analysis. For SEM observations, the samples were coated with carbon, with an average thickness of 200 Å, using a vacuum evaporator JEOL-4 ×. At Luleå University of Technology, Sweden, a high-

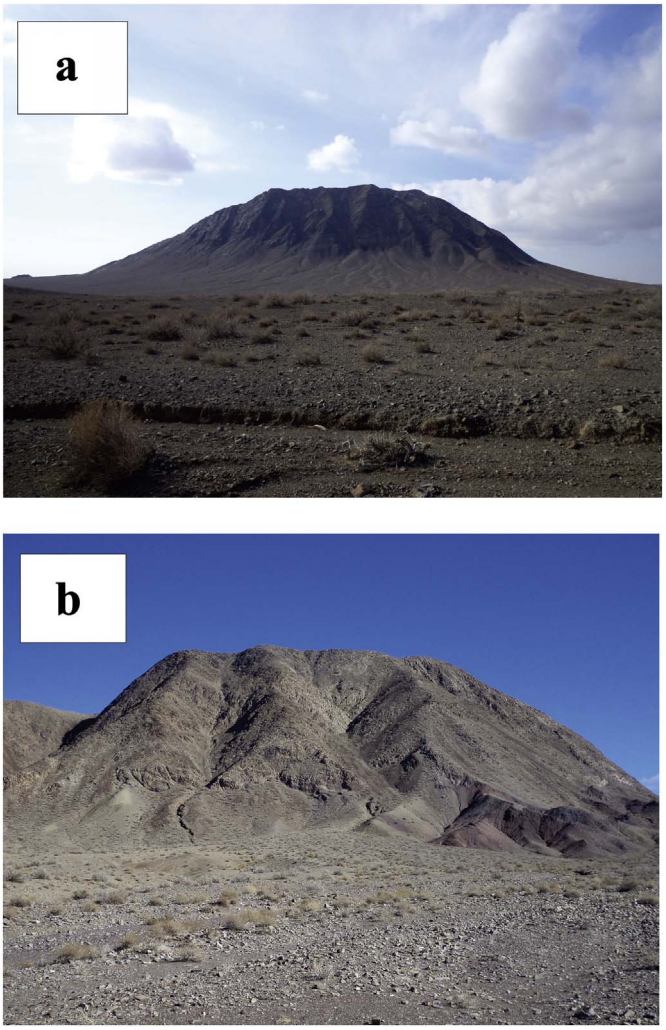


**Fig. 2.** Two intrusions of adakitic rocks. a: Allah Kom dacitic dome. b: Bazmin andesitic dome.

resolution FEG-SEM, Zeiss Merlin, fitted with EDS- and wavelength dispersive spectrometry detectors, was used for backscattered electron imaging (BSE) and complementary EDS element analysis. Analytical settings were 20 kV with a beam current of 1.1 nA. Electron backscattered images were taken in order to investigate potential element zonation in the analyzed minerals.

## 2. Results

### 2.1. Petrography

In the Torud-Ahmad Abad magmatic belt, there are different hypabyssal rocks occurring as domes and dikes. The petrography and geochemical signatures of these rocks have previously been studied (Mansouri Moghaddam, 2014; Jamali, 2014; Yousefi et al., 2016). The rocks include dacite, trachydacite, andesite, trachyandesite, and trachybasaltic andesite, and show porphyritic and glomeroporphyritic textures. Plagioclase, hornblende, and pyroxene (augite) constitute the major minerals of these rocks (Fig. 3). Minor constituents are sericite, chlorite, calcite, apatite and magnetite. The plagioclase crystals are between 2 and 12 mm and show compositional zoning. Some hornblende grains are typically opacitized and some of them show typical optical zoning under polarized light. Based on petrographic observation, the sequence of crystallization in the andesitic and dacitic rocks is pyroxene, amphibole, and plagioclase.

### 2.2. Mineral chemistry

Under this section, results from the analysis by scanning electron microscopy (SEM-EDS) are presented and the more interesting features regarding amphibole, pyroxene, and plagioclase are highlighted.

#### 2.2.1. Amphibole

Amphibole composition can be expressed by the general formula $A_{0-1}B_2C_5T_8O_{22}$ (OH, F, Cl) $_2$, where A=Na, K; B=Na, Zn, Li, Ca, Mn, $Fe^{2+}$, Mg; C=Mg, $Fe^{2+}$, Mn, Al, $Fe^{3+}$, Ti, Zn, Cr; and T=Si, Al, Ti. Amphibole grains from andesitic and dacitic rocks were analyzed for their composition. Fresh amphibole phenocrysts from andesitic and dacitic dikes and domes were analyzed. Results of representative SEM-EDS analyses are presented in Table 1.

To determine what types of amphibole that are present in the rocks of the Torud-Ahmad Abad area, the chemical composition of the amphiboles in the andesitic and dacitic rocks were plotted in a Mg/(Mg + $Fe^{2+}$) vs. Si diagram (Fig. 4a). The amphiboles of the dacitic and andesitic samples plot in the Mg-hornblende field. Based on values of $Al^{VI}$ and $Fe^{3+}$ cations per formula unit, the amphiboles are in the range of pargasite to magnesian-hastingsite (Fig. 4b). $Al^{VI}$ values are higher than $Fe^{3+}$ in pargasite whereas the opposite is observed in hastingsite ($Al^{VI} < Fe^{+3}$). Based on their concentrations of Mg, $Fe^{2+}$, and Si, the studied amphiboles from the trachyandesite, trachydacite and mafic clots plot in the magnesiohornblende to tschermakite fields (Fig. 4c).

The chemical composition of the rims and cores of the analyzed amphibole grains exhibit compositional differences (Table 1). In these rocks, some amphibole crystals display normal and others oscillatory zoning (Fig. 5). Amphibole with normal zoning shows a decrease in $Al^{IV}$, $(Na + K)^A$ and $Fe^{+2}$, and an increase in Mg from core to rim, whereas amphiboles with oscillatory zoning show a rhythmic zonation seen in variations among the element concentrations.

#### 2.2.2. Plagioclase

Plagioclase is the most abundant mineral in the studied rocks. It occurs as phenocrysts, micro-phenocrysts, and microlites. According to the Ab-An-Or diagram by Deer et al. (1996) (Fig. 6), the plagioclase plot mainly in the albite, andesine, and labradorite fields. The percentage of Ab, An, and Or varies in the andesites and dacites ($Ab_{29.15–98.67}$, $An_{0.58–69.26}$ and $Or_{0–7.43}$). Plagioclase commonly displays normal zoning, but reverse and oscillatory zoning are also observed (Fig. 7). Table 2 shows the results of SEM-EDS analyses of plagioclase in the andesites and dacites of the region.

#### 2.2.3. Clinopyroxene

Clinopyroxene grains are < 4 mm in size and euhedral to subhedral. Representative clinopyroxene analyses are provided in Table 3. Most of them plot in the diopside field and some in the augite field in the En-Wo-Fs diagram of Morimoto et al. (1988) (Fig. 8). According to the data, the pyroxenes show only minor compositional variation in Mg, Si, Fe and Al when analyzing from core to rim. In the andesite and basaltic andesite, pyroxene grains show oscillatory zoning (Fig. 9), a phenomenon that will be further discussed below.

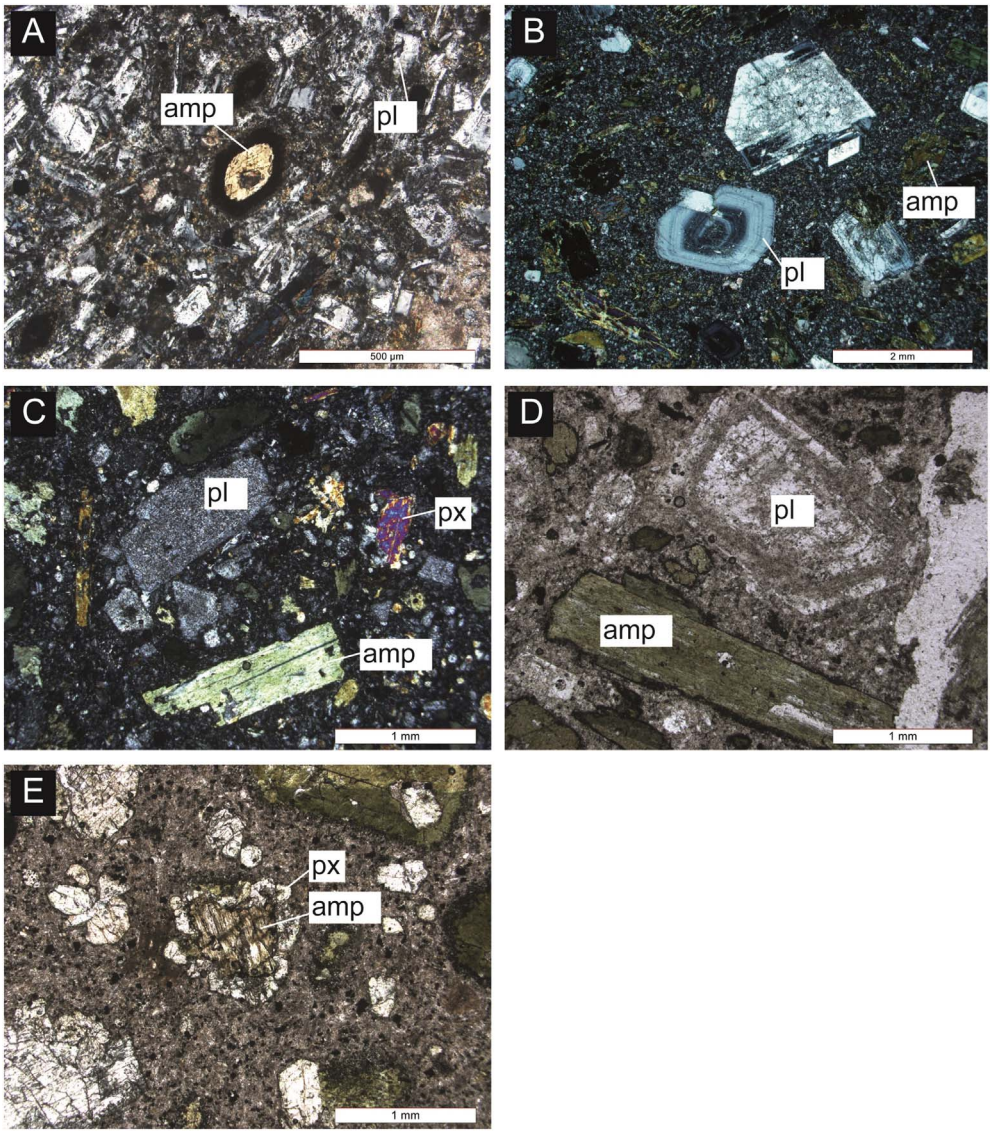


**Fig. 3.** Photomicrographs of the studied rocks (in cross-polarized light). a: porphyritic texture; amphibole and plagioclase phenocrysts within trachydacite; b: plagioclase and amphibole within andesite showing porphyritic texture; c: trachybasaltic andesite with amphibole, pyroxene and plagioclase. d: zoning in plagioclase and amphibole minerals. e: overgrowth texture of pyroxene on amphibole in andesitic rocks. Mineral abbreviations are from Whitney and Evans (2010).

## 3. Discussion

Minerals record magma composition and temperature, formation depth, nature of open system processes, and the rates at which magmas ascend (Putirka, 2008a). Here, the focus will be on mineral chemistry and pressure/temperature calculations of amphibole, pyroxene, and plagioclase, to estimate the depth at which these minerals crystallized and by inference the magma. Based on their chemistry, these minerals have been classified as pargasite/Mg-hastingsite/tschermakite, diopside/augite, and albite/andesine/labradorite, respectively (Figs. 4, 6 and 8).

### 3.1. Mineral zoning

In petrographic studies, zoning is commonly observed in plagioclase and amphibole, and occasionally in pyroxene. Zoning in crystals is interpreted as progressively recording changes in the magmatic environment (Wallace and Bergantz, 2002). Vernon (2008) suggests that compositional zoning is due to local and fast changes of melt composition. Also in andesitic and dacitic rocks, the existence of mineral oscillatory zoning, sieve textures, and crystal dissolution margins indicate changes in temperature, pressure, melt composition, and $fH_2O$ parameters, which generally relate to feeding of the magma chamber with new pulses of magma.

For example, mixing of a hot, mafic magma with more felsic magma containing Na-plagioclase, causes instability of Na-plagioclase leading to the production of Ca-plagioclase around the core (Tsuchiyama, 1985). The overgrowth texture is another interesting feature in the studied minerals. This texture is formed by one mineral rimming another one (Fig. 3e) and may be related to the P, T and compositional change of a new pulse of magma. Lofgren (1974) demonstrated, by using synthetically zoned plagioclase, that the variation in the style of zonation records the physicochemical changes that silicate melts undergo during crystallization. Normal zoning in the studied plagioclase

**Table 1**
Results of SEM-EDS analysis of amphiboles in the hypabyssal andesitic and dactic rocks of the Torud-Ahmadabad magmatic belt. For spot positions of core/rim, see Fig. 5.

| Mineral | Oscillatory-zoned amphibole | | | | | | | | | |
|---|---|---|---|---|---|---|---|---|---|---|
| Host rock position | FR 63 (andesite) | | | | FY 33 (dacite) | | | FR 23 (andesite) | | |
| | Rim | | | Core | Rim | | Core | Rim | | Core |
| $SiO_2$ | 43.2 | 43.35 | 40.76 | 43.66 | 46.32 | 45.6 | 47.76 | 43.76 | 44.5 | 44.45 |
| $TiO_2$ | 1.41 | 0.84 | 0.97 | 0.89 | 1.96 | 2.01 | 1.38 | 1.58 | 1.47 | 1.32 |
| $Al_2O_3$ | 11.42 | 11.94 | 13.9 | 11.96 | 9.55 | 11.35 | 10.77 | 10.72 | 10.97 | 9.88 |
| FeO | 15.29 | 14.32 | 13.96 | 11.57 | 12.54 | 11.71 | 11.4 | 14.77 | 15.77 | 14.42 |
| MnO | 0.54 | 0.48 | 0.24 | 0.25 | – | – | – | 1.06 | – | 0.24 |
| MgO | 10.52 | 10.97 | 12.03 | 14.21 | 13.39 | 12.8 | 12.63 | 11.46 | 11.12 | 11.78 |
| CaO | 12.01 | 11.79 | 11.8 | 11.33 | 10.87 | 12.16 | 12.49 | 11.3 | 11.41 | 12.71 |
| $Na_2O$ | 1.31 | 2.48 | 1.24 | 1.76 | 1.98 | 1.94 | 1.58 | 1.24 | 1.52 | 1.70 |
| $K_2O$ | 1.89 | 1.49 | 1.85 | 1.38 | 0.08 | 0.42 | 0.22 | 0.99 | 0.88 | 1.19 |
| $Cr_2O_3$ | – | – | 0.26 | 0.21 | 0. 40 | 0.23 | 0.01 | 0.16 | – | 0.31 |
| Total | 97.59 | 97.66 | 97.01 | 97.22 | 97.07 | 98.22 | 98.24 | 97.04 | 97.64 | 98.00 |
| Structural formula (Leake et al., 1997) | | | | | | | | | | |
| Si | 6.48 | 6.48 | 6.02 | 6.34 | 6.70 | 6.61 | 6.68 | 6.45 | 6.55 | 6.61 |
| Al iv | 1.97 | 1.51 | 1.51 | 1.65 | 1.38 | 1.29 | 1.13 | 1.54 | 1.44 | 1.38 |
| Al vi | 0.49 | 0.58 | 0.45 | 0.39 | 0.33 | 0.55 | 0.68 | 0.32 | 0.45 | 0.34 |
| Ti | 0.15 | 0.09 | 0.10 | 0.09 | 0.21 | 0.21 | 0.14 | 0.17 | 0.16 | 0.14 |
| Cr | – | – | 0.03 | 0.02 | 0.04 | 0.02 | 0.01 | 0.01 | – | 0.03 |
| $Fe^{3+}$ | 0.10 | – | 0.82 | 0.76 | 0.54 | – | – | 0.72 | 0.54 | – |
| $Fe^{2+}$ | 1.81 | 1.79 | 0.89 | 0.63 | 1.41 | 1.36 | 0.97 | 1.79 | 1.39 | 1.09 |
| Mn | 0.06 | 0.06 | 0.03 | 0.01 | – | – | – | 0.13 | – | 0.03 |
| Mg | 2.35 | 2.65 | 2.44 | 3.07 | 2.80 | 2.76 | 2.8 | 2.44 | 2.52 | 2.61 |
| Ca | 1.93 | 1.88 | 1.87 | 1.76 | 1.68 | 1.88 | 1.92 | 1.78 | 1.80 | 2.02 |
| Na | 0.38 | 0.71 | 0.35 | 0.49 | 0.55 | 0.54 | 0.44 | 0.35 | 0.35 | 0.49 |
| K | 0.35 | 0.28 | 0.34 | 0.24 | 0.01 | 0.07 | 0.04 | 0.18 | 0.16 | 0.22 |

suggests a change from a high-temperature labradorite composition in the core to a lower-temperature albite composition at the rim (Figs. 6, 7). Reverse zoning indicates disequilibrium conditions and a return to less-evolved compositions. Oscillatory zoning is a repetitive, more or less periodic variation in plagioclase composition. Pringle et al. (1974) conclude that oscillatory growth is controlled by the changing composition of the melt at the crystal-melt interface.

Hewinz (1974) studying a rare and complex core and rim relation in augite state that the differences in composition of pyroxene show a pyroxene fractionation trend, where the cores are richer in Mg and Si and poorer in Fe, Ti and Al than the rims and also suggest that the changes were due to increase in Ca and possibly an increase in $fO_2$, and that may appear just due to evolution in the crystal pile. Claeson et al. (2007) suggest that the sector zonation observed optically corresponds most closely to variations in $TiO_2$ and $Al_2O_3$. The cause of sector zoning in clinopyroxene may be related to differences in atomic structure and/or growth mechanisms. Most models for sector zoning in clinopyroxene have invoked high crystal growth rates as the fundamental cause. Based on mineral chemistry data, it can be seen that some of the presently studied pyroxene grains show oscillatory zoning (Fig. 9). This zoning shows that the crystallization environment was variable in terms of composition, temperature, and pressure. Couch et al. (2001) believe that the mixing of two magmatic pulses in a magma chamber causes a change in the total magma composition (e.g. a change in the amount of $TiO_2$, MnO, CaO, and MgO). In the samples studied here, some pyroxenes, $TiO_2$ and MnO show opposite trends while CaO and MgO show the same trend. In some samples, the amount of $Al_2O_3$ increases from core to rim, proposing evolution of the magma by crystallization. These features can be attributed to for instance changes in parameters such as temperature, pressure, $f$H2O, and the composition of the melt (Foley et al., 2013). The change in major element composition from core to rim indicates a magma mixing might have occurred during the ascending of magma and intrusion of a new pulse of magma. The mafic clots constitute evidence for mixing of two magmatic pulses (Yousefi et al., 2017).

An interesting feature observed in some of the studied amphibole grains is the opacity phenomenon (Fig. 3a). The opacity phenomenon is the result of an imbalance of hydrous minerals in an anhydrous environment at high temperature under the influence of exothermic processes (Middlemost, 1986). Rutherford and Devine (2003) attributed the opacity phenomenon to the rapid decrease of pressure. Furthermore, the reaction rim of clinopyroxene seen on the igneous amphibole phenocryst in Fig. 3e is an indication that at some point the magma temperature was brought above the hornblende stability field, forming the clinopyroxene rim. Rutherford and Devine (2003) showed that this texture may be reproduced experimentally and is developed in a very short time span, in hours to days.

### 3.2. P-T conditions

#### 3.2.1. Thermobarometry of amphibole

Pressure and temperature estimates of these rocks are based on geothermobarometry of amphibole and clinopyroxene. For the estimation of pressure, one of the most common geobarometers used is the amount of aluminum in the structure of amphibole (e.g., Hammarstrom and Zen, 1986; Hollister et al., 1987; Johnson and Rutherford, 1989; Schmidt, 1992; Holland and Blundy, 1994; Anderson and Smith, 1995; Ridolfi et al., 2010; Ridolfi and Renzulli, 2012). Accordingly, it is possible to use this geobarometer to determine the depth of the magma emplacement (e.g., Vyhnal et al., 1991). Using the formula of Ridolfi and Renzulli (2012), it is possible to estimate the P-T conditions and $fO_2$ for a wide range of physicochemical conditions for calc-alkaline and alkaline magmas (e.g., 800–1130 °C, 1.3–22 kbar), with a low uncertainty (T ± 23.5 °C, P ± 11.5%).

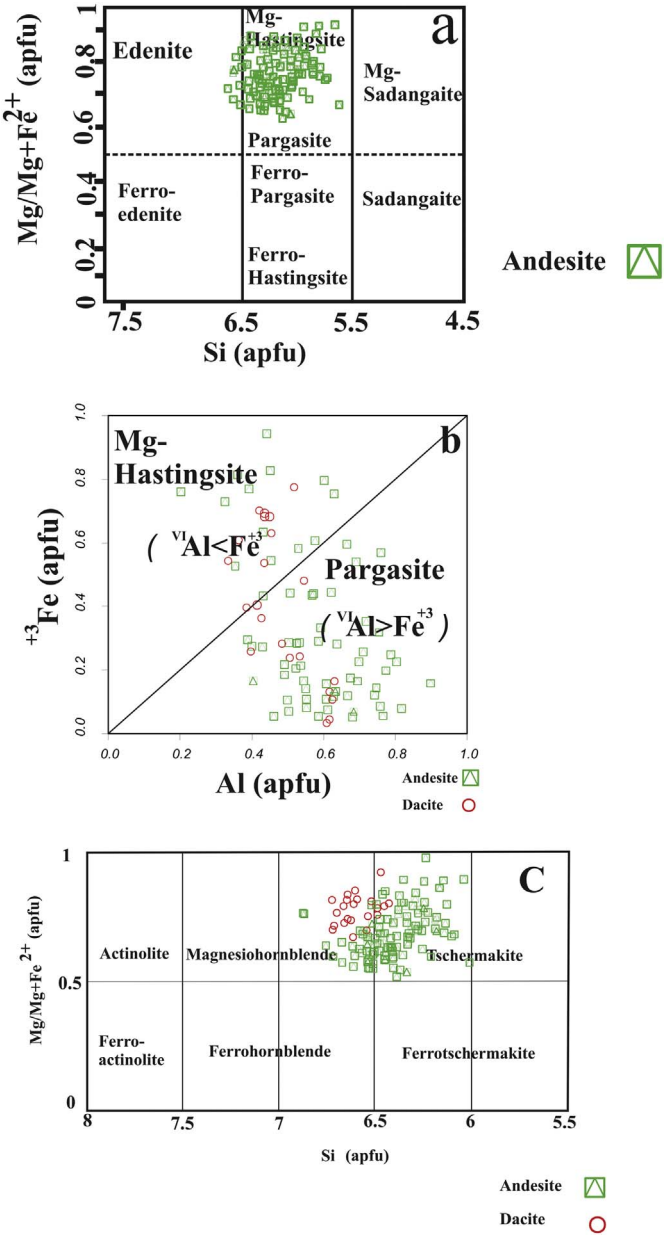


**Fig. 4.** Classification diagrams for amphibole (Leake et al., 1997, 2004).a: amphiboles in the high-magnesium andesitic samples plot between pargasite and Mg-hastingsite field. b: amphiboles in andesites and dacites with $Al^{VI} > Fe^{3+}$ and $Al^{VI} < Fe^{3+}$ plot between the pargasite and Mg-hastingsite field c: the range of amphibole compositions of trachyandesite, trachydacite, and mafic clots in the $Mg/(Mg + Fe^{2+})$ vs. Si diagram.

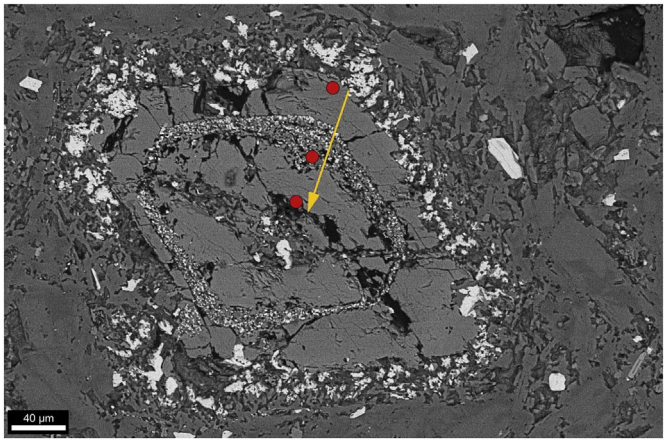


**Fig. 5.** Backscattered electron image of an amphibole crystal with normal zoning. SEM-EDS spots are shown as red dots and the arrow direction shows the order in which the spots were analyzed, which is also indicated in Table 1. (For interpretation of the references to colour in this figure legend, the reader is referred to the web version of this article.)

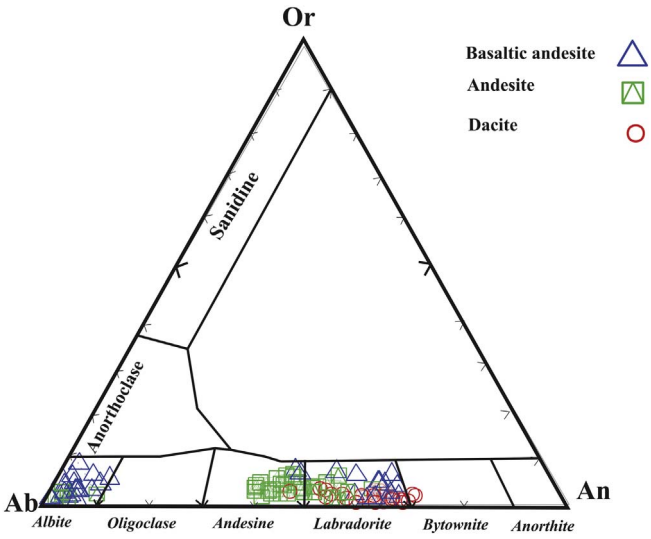


**Fig. 6.** Ab-An-Or ternary plot for plagioclase compositions.

Calculations for the analyzed amphiboles show that the crystallization of Mg-hastingsite and tschermakitic amphibole in andesites of the Torud-Ahmad Abad magmatic belt took place at a temperature of about 850–1030 °C, with the highest frequency at 1030 °C, under a lithostatic pressure of 2–6 kbar, with the highest frequency at 6 kbar (Figs. 10, 11). Mg-hornblendes in dacite crystallized at temperatures of 920 to 970 °C, with most data gathering between 940 and 960 °C, at pressure conditions of 3–4.5 kbar (Figs. 10, 11). The chemistry of amphibole in mafic clots (pyroxene and amphibole clots), suggests a temperature range of 500–800 °C and a pressure of 4.2–8.2 kbar, with highest frequency of data close to 680 °C and 6.2 kbar. Since the thermometer used here provides reliable temperature estimates in the range of 800 to 1130 °C (Ridolfi and Renzulli, 2012), the low temperatures for the amphibole/pyroxene in the mafic clots may indicate reactions with the enclosing magma composition and therefore not register any significant igneous data.

The amphibole data combined indicate an upper pressure limit of c. 6 kbar, at c. 1030 °C. With regard to the relation between depth and pressure (Putirka et al., 2003), the depth of magma crystallization in the studied rocks occurred at a crustal depth of approximately < 30 km.

### 3.2.2. Thermobarometry of pyroxene

Two methods from Putirka et al. (2003) and Putirka (2008b) were used for calculating the P-T conditions of clinopyroxene crystallization. The first thermobarometer is based on equations in Putirka et al. (2003), which suggests pyroxene crystallization temperatures at

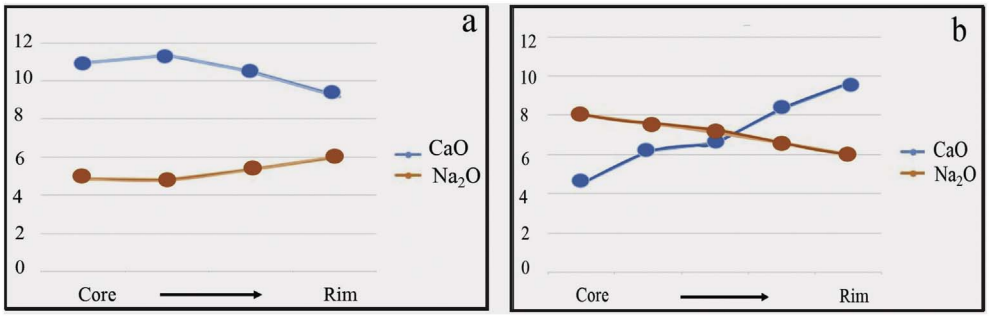


**Fig. 7.** Variations from core to rim in plagioclase composition of andesitic rocks. a: normal-zoned plagioclase. b: reverse-zoned plagioclase.

**Table 2**
Results of SEM-EDS analysis of plagioclase in the hypabyssal rocks of the Torud-Ahmad Abad magmatic belt. For spot positions of core/rim, see Fig. 6.

| Mineral | Normal-zoned plagioclase | | | | Oscillatory-zoned plagioclase | | | | | | Reverse zoned plagioclase | | | | |
|---|---|---|---|---|---|---|---|---|---|---|---|---|---|---|---|
| Host rock position | FR 63 (Andesite) | | | | FR23 (Andesite) | | | | | | Fy33 (Dacite) | | | | |
| | Core | | | Rim | Rim | | | | | Core | Core | | | | Rim |
| $SiO_2$ | 53.92 | 54.19 | 54.89 | 56.33 | 54.08 | 58.98 | 52.43 | 56.05 | 55.98 | 55.46 | 63.36 | 62.23 | 59.95 | 58.27 | 57.23 |
| $Al_2O_3$ | 28.22 | 28.99 | 28.46 | 27.09 | 28.48 | 25.59 | 30.03 | 27.11 | 27.6 | 27.74 | 22.7 | 23.6 | 23.6 | 25.6 | 26.3 |
| FeO | 0.56 | 0.36 | – | 0.46 | 0.18 | 0.05 | 0.26 | 0.56 | – | 0.4 | 0.6 | 0.3 | 1.68 | 0.8 | 0.5 |
| CaO | 10.95 | 11.34 | 10.48 | 9.27 | 10.65 | 7.31 | 12.44 | 9.78 | 9.65 | 10.46 | 4.5 | 6.2 | 6.6 | 8.3 | 9.6 |
| $Na_2O$ | 4.87 | 4.83 | 5.36 | 5.99 | 4.99 | 7.02 | 4.13 | 5.58 | 5.63 | 5.21 | 8.0 | 7.6 | 7.3 | 6.6 | 6.0 |
| $K_2O$ | 0.45 | 0.48 | 0.32 | 0.49 | 0.52 | 0.6 | 0.49 | 0.53 | 0.68 | 0.57 | 0.8 | – | 0.57 | 0.5 | 0.3 |
| BaO | 0.31 | 0.09 | 0.21 | – | 0.57 | 0.22 | 0.05 | 0.15 | 0.16 | – | 0.0 | – | 0.21 | – | 0.0 |
| Total | 99.27 | 100.28 | 99.72 | 99.63 | 99.48 | 99.76 | 99.82 | 99.76 | 99.71 | 99.84 | 100.0 | 99.9 | 100.1 | 100.0 | 100.0 |
| Feldspar component | | | | | | | | | | | | | | | |
| Or | 3.14 | 2.92 | 2.22 | 2.79 | 4.05 | 3.8 | 2.91 | 3.34 | 4.18 | 3.29 | 4.5 | – | 3.69 | 2.64 | 1.65 |
| Ab | 43.19 | 42.23 | 46.98 | 52.4 | 44 | 61.06 | 36.4 | 49.09 | 49.19 | 45.82 | 72.7 | 68.9 | 64.46 | 57.5 | 52.2 |
| An | 53.56 | 54.83 | 50.79 | 44.8 | 51.9 | 35.12 | 60.7 | 47.56 | 46.61 | 50.88 | 22.7 | 31.1 | 31.8 | 39.9 | 46.1 |

**Table 3**
Compositional SEM-EDS data for clinopyroxenes in the hypabyssal rocks of the Torud-Ahmad Abad magmatic belt. For spot positions of core/rim, see Fig. 7.

| Mineral | FR32 (basaltic andesite) | | | | FR 11 (andesite) | | | | | | FR 11 (andesite) | | |
|---|---|---|---|---|---|---|---|---|---|---|---|---|---|
| Host rock position | Oscillatory-zoned pyroxene | | | | | | | | | | | | |
| | Rim | | | Core | Rim | | | | | Core | Rim | | Core |
| $SiO_2$ | 51.73 | 51.54 | 51.74 | 51.3 | 51.39 | 52.06 | 51.75 | 52.48 | 51.92 | 52.01 | 52.08 | 52.48 | 51.46 |
| $TiO_2$ | – | 0.54 | 0.88 | 0.35 | 0.85 | 1.18 | 0.25 | 0.52 | 0.32 | 0.88 | 0.74 | 0.34 | 0.67 |
| $Al_2O_3$ | 4.06 | 3.19 | 3.45 | 4.78 | 2.62 | 2.05 | 2.06 | 1.96 | 2.02 | 2.48 | 0.84 | 1.12 | 2.32 |
| FeO | 4.24 | 4.44 | 4.86 | 6.18 | 8.27 | 8.23 | 10.26 | 9.94 | 10.79 | 9.75 | 8.57 | 8.99 | 10.01 |
| MnO | – | 0.4 | 0.32 | 0.28 | 0.49 | – | 0.19 | 0.32 | 0.76 | 0.47 | 0.6 | 0.63 | 0.67 |
| MgO | 14.88 | 14.97 | 14.5 | 13.79 | 14.16 | 14.23 | 11.84 | 13.33 | 13.09 | 12.84 | 15.32 | 13.99 | 12.9 |
| CaO | 23.98 | 23.06 | 23.84 | 23.62 | 21.61 | 21.64 | 23.57 | 21.07 | 20.33 | 20.83 | 21.13 | 21.87 | 21.76 |
| $Na_2O$ | 0.06 | 0.76 | 0.26 | – | 0.4 | 0.53 | – | 0.54 | 0.3 | 0.71 | – | 0.05 | 0.06 |
| $K_2O$ | 0.07 | 0.39 | – | 0.049 | 0.059 | 0.04 | 0.44 | – | 0.2 | – | 0.02 | 0.09 | 0.16 |
| $Cr_2O_3$ | 0.82 | – | 0.32 | – | 0.01 | 0.091 | – | – | 0.26 | 0.05 | 0.43 | 0.17 | 0.08 |
| Total | 99.88 | 99.34 | 100.2 | 100.39 | 99.92 | 100.07 | 100.4 | 100.2 | 100.03 | 100.08 | 99.82 | 99.76 | 100.13 |
| Pyroxene component (%) | | | | | | | | | | | | | |
| En | 43.13 | 43.69 | 41.97 | 40.09 | 40.9 | 41.36 | 34.17 | 38.93 | 38.27 | 38.27 | 42.97 | 39.84 | 37.36 |
| Fs | 6.89 | 7.94 | 8.42 | 10.56 | 14.22 | 13.42 | 16.93 | 16.83 | 18.98 | 17.1 | 14.44 | 15.39 | 17.35 |
| Wo | 49.96 | 48.35 | 49.6 | 49.34 | 44.87 | 45.2 | 48.88 | 44.22 | 42.73 | 44.61 | 42.57 | 44.75 | 45.28 |

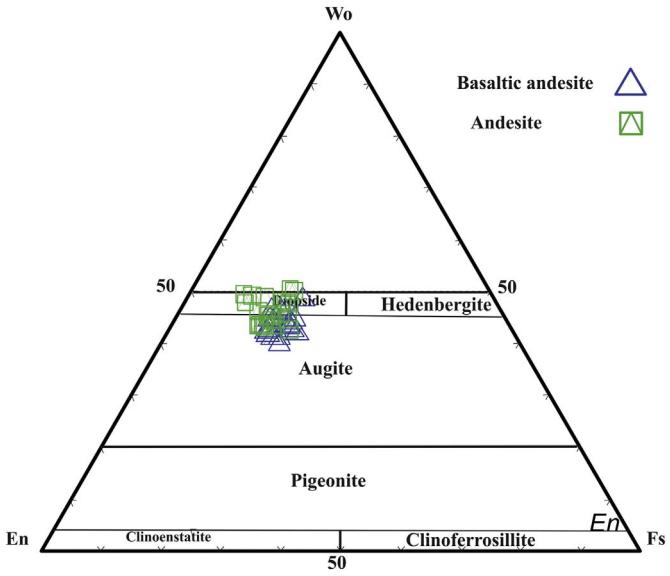


**Fig. 8.** En–Wo–Fs ternary diagram for determination of clinopyroxene.

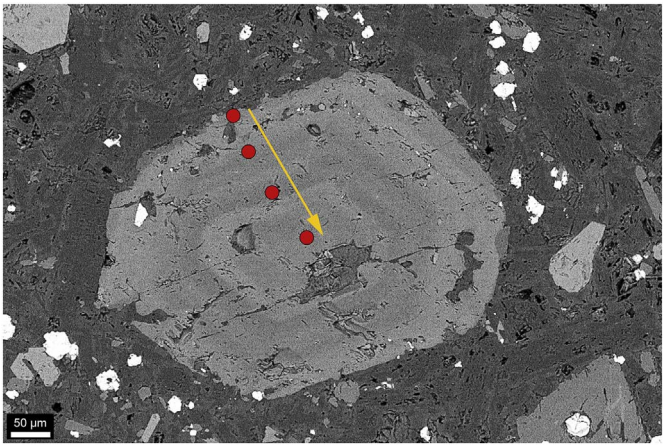


**Fig. 9.** Representative backscattered electron image of a clinopyroxene grain displaying oscillatory zoning. SEM-EDS spots are shown as red dots and the arrow direction represents the order the spots were analyzed, as indicated in Table 1. (For interpretation of the references to colour in this figure legend, the reader is referred to the web version of this article.)

989–1213 °C and a pressure range of 1–11 kbar. The second method given by Putirka (2008b) generates a temperature estimate determined without the involvement of liquid composition, and the standard error of estimation for this method is ± 1.5 kbar. This method indicate pyroxene crystallization at about 1020 to 1170 °C, with the highest frequency at 1050 °C, and a pressure of 2–10 kbar, with the highest frequency at 9 kbar for basaltic andesite samples (Fig. 11). These P-T settings are in agreement with data reported by e.g. Martin (2007) and Sen (1985). It should be noted that the results of different geothermobarometers should be consistent with each other and with petrographic evidence. Here, frequency histograms are used for illustrating the range of variation and frequency of the temperature and pressure for crystallization of pyroxene and amphibole. Some of the lower temperature and pressure values likely suggest a re-equilibration during cooling and ascent of the magma.

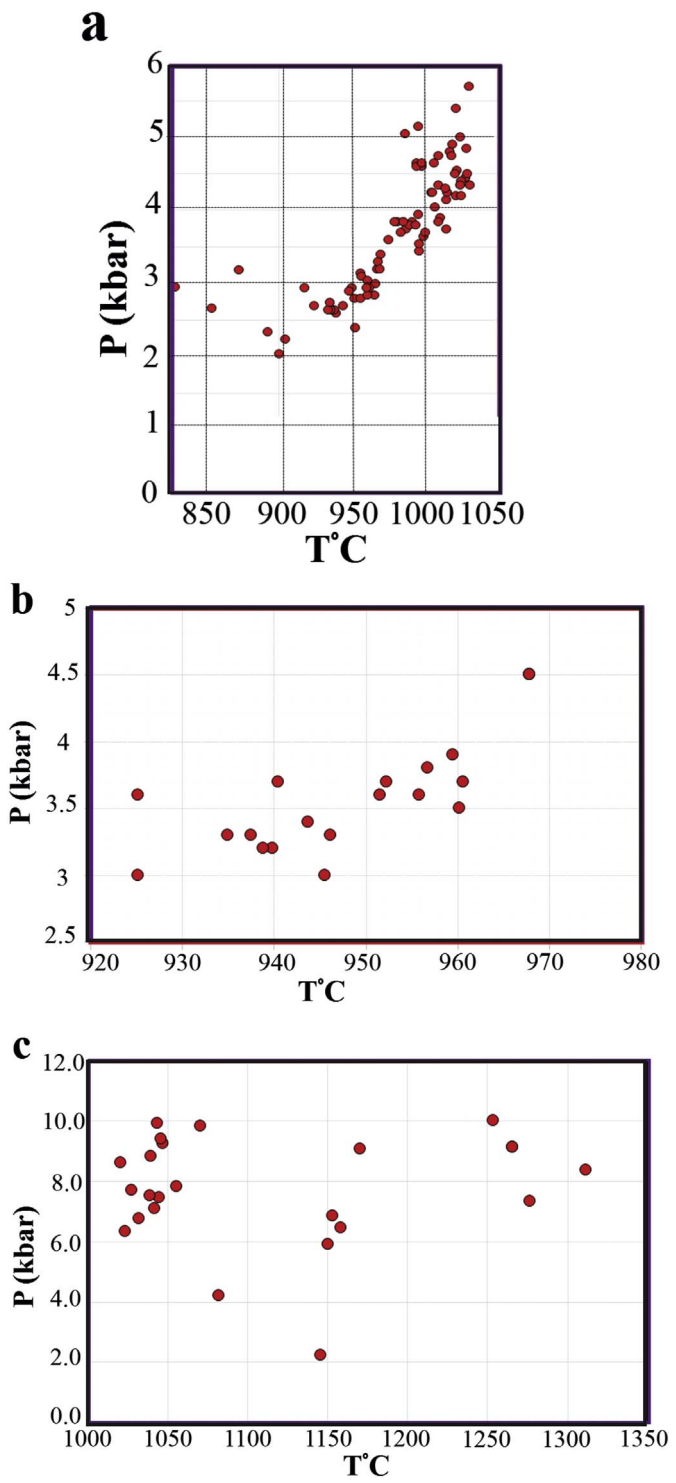


**Fig. 10.** P-T data for amphibole in dacite and andesite. a): diagram for andesite, b): diagram for dacite, c): P-T diagram for clinopyroxene (diopside-augite) of basaltic andesite (Ridolfi and Renzulli, 2012).

In addition to the P-T estimation, the mineral chemistry of amphiboles can be used to determine the tectonomagmatic environment (Leake, 1971). Amphiboles with 6–7 values per formula Si (Table 1) are

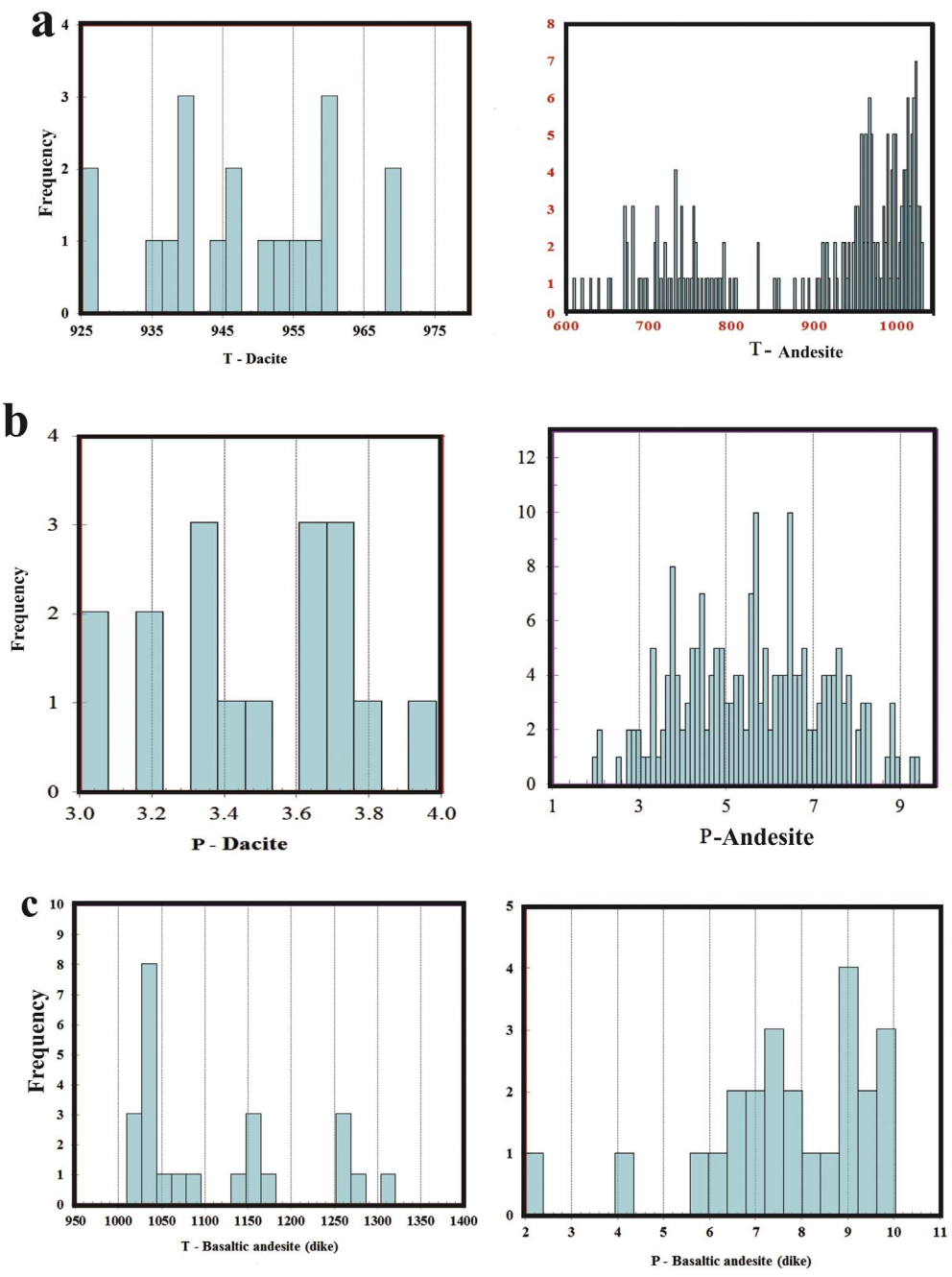


**Fig. 11.** Frequency histograms of the temperature and pressure of crystallization of amphibole (hornblende). a: Temperature of crystallization of minerals in andesite and dacite. b: Pressure of crystallization of minerals in andesite and dacite. c: P-T of crystallization of minerals (pyroxene) in basaltic andesites.

characteristic of igneous amphiboles (Leake, 1978). As shown in Fig. 12a, the analyzed amphiboles plot in the igneous amphibole field. According to the diagram of Coltorti et al. (2007), these amphiboles are related to a subduction environment (I-amph: Interplate and S-amph: Subduction) (Fig. 12b).

Based on the thermobarometric data above, amphibole and pyroxene mineral chemistry suggests a magmatic crystallization depth of < 33 km. In Iran, the depth to Moho varies (Dehghani and Makris, 1983; Mooney, 1998; Jamshidi et al., 2015). Motaghi et al. (2012) suggest a large variation of the Moho depth, from 35 km under central Iran, to 55 km beneath the northeastern parts of the country. According to Taghizadeh-Farahmand et al. (2014), the average Moho depth beneath central Iran, varies between 42 and 46 km.

Petrographic evidence and mineral chemical data from this study

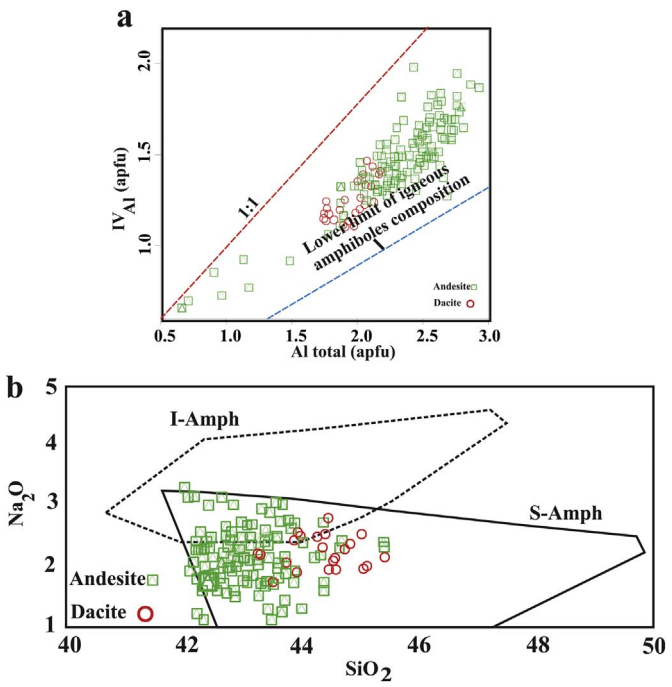


**Fig. 12.** a. Diagram for determining amphibole magmatic series (Leake, 1971). b. Diagram of Coltorti et al. (2007), indicating that the amphiboles are associated with subduction.

corroborate the findings by Yousefi et al. (2016, 2017), and indicate that the parent magma of the high-silica adakitic domes originated from the melting of a subducted metamorphosed Neo-Tethyan oceanic slab (Sabzevar–Darouneh branch). The low-silica adakite in Sahl-Razzeh was formed by partial melting of a metasomatized or modified mantle wedge above a subducted oceanic slab (Fig. 13).

## 4. Conclusion

The Torud-Ahmad Abad magmatic belt, Iran, formed in a subduction zone environment, in a volcanic arc tectonic setting. The hypabyssal rocks, or domes, are composed of basaltic trachyandesite, trachyandesite, trachydacite and dacite with adakitic feature. Amphibole, plagioclase and pyroxene are the main minerals in these rocks. Geothermobarometric calculations show that the Mg-hastingsite and tschermakitic amphibole in the andesite rocks crystallized at a temperature range of about 850–1030 °C, with the highest data frequency at ca. 1030 °C, under a lithostatic pressure of 2–6 kbar, with most data at ca. 6 kbar. Magnesian-hornblende in dacitic rocks crystallized at 920–970 °C, at a pressure of 3–4.5 kbar. Geothermobarometry of pyroxene in basaltic andesite show that the crystallization of magma initiated at temperatures from 1020 to 1170 °C, at pressure conditions of 2.2–9.8 kbar.

Based on the results of pressure and temperature, the depth of magma crystallization is estimated to be < 30 to 30 km. The studied magmatic rocks are related to subduction of the Sabzevar–Darouneh Neo-Tethyan oceanic slab beneath the continental crust of the northern part of the Central Iran Structural Zone.

## Acknowledgements

The authors gratefully acknowledge Dr Dick T. Claeson, Dr Martiya Sadeghi and Dr Ghasem Ghorbani for their constructive comments that significantly improved the original manuscript.

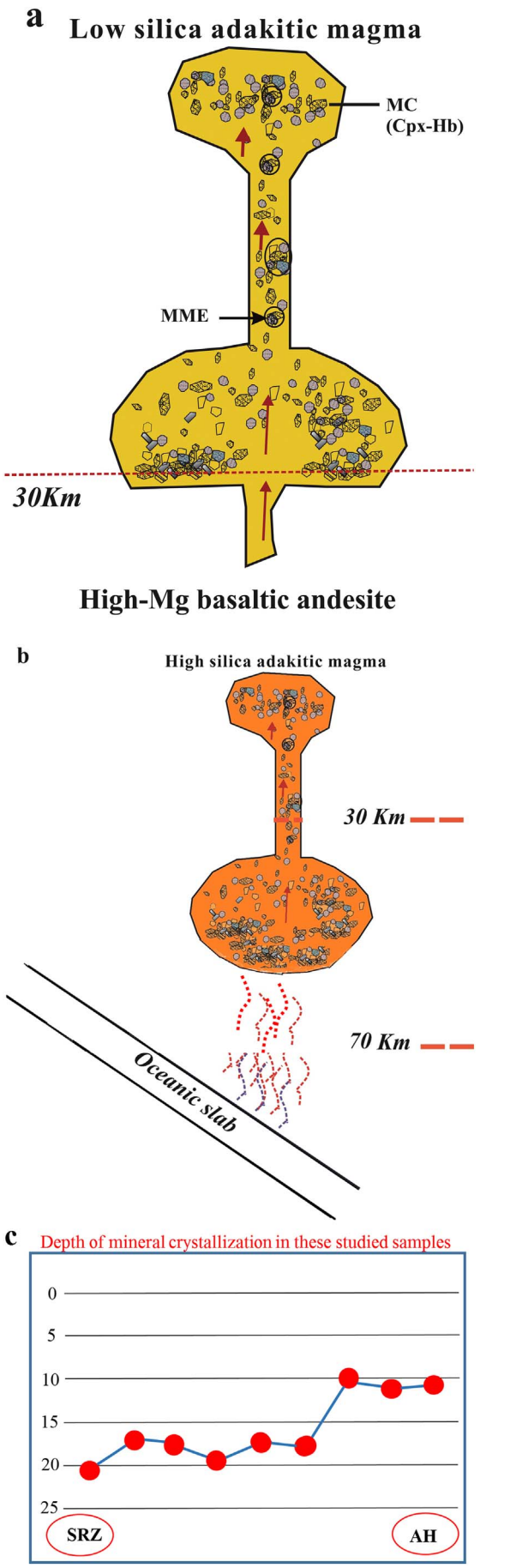


(caption on next page)

**Fig. 13.** Schematic design of crystallization of minerals in magma chamber. a. mineral crystallization in low silica adakitic magma and high silica adakitic magma b. (MME: Mafic Micro granular Clot and MC: Mafic Clot). c. Calculated depth of mineral crystallization in high silica adakitic magma and low silica adakitic magma (SRZ: Sahl-Razze region and AH: Ahmad Abad region).

## References


Abbott Jr., R.N., Clarke, D.B., 1979. Hypothetical liquidus relationships in the subsystem $Al_2O_3$–FeO–MgO projected from quartz, alkali feldspar and plagioclase for a ($H_2O$) 61. Can. Min. J. 17, 549–560.

Anderson, J.L., Smith, D.R., 1995. The effects of temperature and $FO_2$ on the Al-in-hornblende barometer. J. American Mineralogist 80, 549–559 No. 5–6.

Blundy, J.D., Shimizu, N., 1991. Trace element evidence for plagioclase recycling in calcalkaline magmas. J. Earth. Planet. Sci. Lett. 102, 178–197.

Claeson, D.T., Meurer, W.P., Hogmalm, K.J., Larson, S.A., 2007. Using LA-ICPMS mapping and sector zonation to understand growth and trace-element partitioning in sector-zoned clinopyroxene oikocrysts from the Norra Ulvö Gabbro, Sweden. J. Petrol. 48, 711–728.

Coltorti, M., Bonadiman, C., Faccini, B., Grégoire, M.O., Reilly, S.Y., Powell, W., 2007. Amphiboles from suprasubduction and intraplate lithospheric mantle. J. Aust. Lit. 99, 68–84.

Couch, S., Sparks, R.S.1., Carroll, M.R., 2001. Mineral disequi librium in lavas explained by convective self-mixing in open magma chambers. J. Nature 411, 1037–1039.

Darvishzadeh, A., 2004. Geology of Iran. Amir Kabir Publications, Tehran, pp. 434 (In Persian).

Deer, W.A., Howie, R.A., Zussman, J., 1996. An Introduction to Rock-forming Minerals, 17th Edition. Longman Ltd., London, pp. 528.

Dehghani, G.A., Makris, J., 1983. The gravity field and crustal structure of Iran. In: Geodynamic Project (Geotraverse) in Iran. Geological Survey of Iran, Final Report number 51. pp. 50–68.

Foley, F., Norman, J., Pearson, N.J., Rushmer, T., Turner, S., Adam, J., 2013. Magmatic evolution and magma mixing of Quaternary adakites at Solander and little Solander Islands, New Zealand. J. Petrol. 54, 1–42.

Ghasemi, H., Rezaei Kahkhaei, M., 2015. Petrochemistry and tectonic setting of the Davarzan Abbasabad Eocene Volcanic (DAEV) rocks, NE Iran. J. Mineral. Petrol. 6, 235–252.

Hammarstrom, J.M., Zen, E., 1986. Aluminum in hornblende: an empirical igneous geobarometer. J. Am. Mineral. 71, 1297–1313.

Helmy, H.M., Ahmed, A.F., El Mahallawi, M.M., Ali, S.M., 2004. Pressure, temperature and oxygen fugacity conditions of calc-alkaline granitoids, Eastern Desert of Egypt, and tectonic implications. J. Afr. Earth Sci. 38, 255–268.

Hewinz, R.H., 1974. Pyroxene crystallization trends and contrasting augite zoning in the Sudbury nickel lrruptive. J. Am. Mineral. 59, 120–126.

Holland, T., Blundy, J., 1994. Non-ideal interactions in Cal-cic amphiboles and their bearing on amphibole-Pla-gioclase thermometry. J. Contrib. Mineral. Petrol. 116, 433–447.

Hollister, L.S., Grissom, G.C., Peters, E.K., Stowell, H.H., Sisson, V.B., 1987. Confirmation of the empirical correlation of Al in hornblende with pressure of solidification of clac-alkaline plutons. J. Am. Mineral. 72, 231–239.

Jamali, Z., 2014. Geology, Petrology and Geochemistry of Subvolcanic Domes of Razzeh Area (South of Shahrood). MSc thesis. University of Shahrood, Shahrood, Iran, pp. 169 in Persian.

Jamshidi, K., Ghasemi, H., Troll, V.R., Sadeghian, M., Dahren, B., 2015. Magma storage and plumbing of adakite-type post-ophiolite intrusion in the Sabzevar ophiolitic zone, northern Iran. J. Solid Earth. 6, 49–72.

Johnson, M.C., Rutherford, M.J., 1989. Experimental calibration of the aluminum-in-hornblende geobarometer with applications to Long Valley Caldera (California) volcanic rocks. J. Geol. 17, 837–841.

Leake, B.E., 1971. On aluminous and edenitic hornblendes. Mineral. Mag. 38, 389–407.

Leake, B.E., 1978. Nomenclature of amphiboles. J. Am. Mineral. 63, 1023–1052.

Leake, B.E., Woolley, A.R., Arps, C.E.S., Birch, W.D., Gilbert, M.C., Grice, J.D., Hawthorne, F.C., Kato, A., Kisch, H.J., Krivovichev, V.G., Linthout, K., Laird, J., Mandarino, J.A., Maresch, W.V., Nickel, E.H., Rock, N.M.S., Schumacher, J.C., Smith, D.C., Stephenson, N.C.N., Ungaretti, L., Whittaker, E.J.W., Youzhi, G., 1997. Nomenclature of amphiboles: report of the subcommittee on amphiboles of the international mineralogical association, commission on new minerals and mineral names. J. Am. Mineral. 82, 1019–1037.

Leake, B.E., Wooley, A.R., Birch, W.D., Burke, E.A.J., Ferraris, G., Grice, J.D., Hawthorne, F.C., Kisch, H.J., Krivovichev, V.G., Schumacher, J.C., Stephenson, N.C.N., Whittaker, E.J.W., 2004. Nomenclature of amphiboles: additions and revisions to the international mineralogical associations amphibole nomenclature. J. Am. Mineral. 89, 883–887.

Lofgren, G., 1974. Temperature induced zoning in synthetic plagioclase feldspar. In: Mackenzie, W.S., Zussman, J. (Eds.), The feldspars. J. Manchester University Press, pp. 362–375.

Mansouri Moghaddam, B., 2014. Petrology and Geochemistry of Subvolcanic Domes in Southeast of Sahl Area (NE Torud). MSc thesis. University of Shahrood, Shahrood, Iran in Persian. p. 119.

Martin, R.F., 2007. Amphibole in the igneous environment. J. Rew. Mineral. Geochem. 67, 323–358.

Middlemost, E.A., 1986. Magmas and Magmatic Rocks: An Introduction to Igneous Petrology.

Moeinvaziri, H., 1996. The History of Magmatism in Iran. Tarbiat Moallem University Publication, Tehran, pp. 440 (In Persian).

Mooney, W.D., 1998. A global model at 5° * 5°. J. Geophys. Res. 103, 727–747.

Morimoto, N., Fabries, J., Ferguson, A.K., Ginzburg, I.V., Ross, M., Seifert, F.A., Zussman, J., Aoki, K., Gottardi, G., 1988. Nomenclature of pyroxenes. J.Am. Mineral. 173, 1123–1133.

Motaghi, K., Tatar, M., Shomali, Z.H., Kaviani, K., Priestley, K., 2012. High resolution image of uppermost mantle beneath NE Iran continental collision zone. J. Phys. Earth Planet. Inter. 208, 38–49.

Nabavi, M.H., 1976. The History of Geology of Iran. Geological Survey of Iran Publication, Tehran, pp. 109 (In Persian).

Nezafati, N., 2015. Mineral resources of Iran; an overview. In: 66 of Conference of Berg- und Hüttenmännischer Tag (BHT). Volume: 66. pp. 1–33 At Freiberg, Germany.

Pringle, G.J., Trembath, L.T., Pajari, G.E., 1974. Crystallization history of a zoned plagioclase. J. Mineral. Mag. 39, 867–877.

Putirka, K.D., 2008a. Introduction to minerals, inclusions and volcanic processes. J. Mineral. Geochem. 69, 1–8.

Putirka, K.D., 2008b. Thermometers and barometers for volcanic systems. In: Putrika, K., Tepley, F. (Eds.), Minerals, inclusions and volcanic processes. Rev. J. Mineral. Geochem. 69. pp. 61–120.

Putirka, K.D., Mikaelian, H., Ryerson, F., Shaw, H., 2003. New clinopyroxene-liquid thermobarometers for mafic, evolved, and volatile-bearing lava compositions, with applications to lavas from Tibet and the Snake River Plain. Idaho. J. Am. Mineral. 88, 1542–1554.

Rahmati Ilkhchi, M., 2009. Metamorphism and geotectonic position of the Shotur Kuh complex, central Iranian block (PhD Thesis). Charles University, pp. 119.

Ridolfi, F., Renzulli, A., 2012. Calcic amphiboles in calc-alkaline and alkaline magmas: thermobarometric and chemometric empirical equations valid up to 1130 °C and 2.2 GPa. Contrib. J. Mineral. Petrol. 163, 877–895.

Ridolfi, F., Renzulli, A., Puerini, M., 2010. Stability and chemical equilibrium of amphibole in calc-alkaline magmas: an overview, new thermobarometric formulations and application to subduction-related volcanoes. J. Contrib. Mineral. Petrol. 160, 45–66.

Rutherford, M.J., Devine, A.D., 2003. Magmatic conditions and magma ascent as indicated by Hornblende phase equilibria and reaction in the 1995–2002, Soufriere Hills Magma. J. Petrol. 44, 1433–1484.

Schmidt, M.W., 1992. Amphibole composition in tonalite as a function of pressure an experimental calibration of the Al-hornblende barometer. J. Contrib. Mineral. Petrol. 110, 304–310.

Sen, G., 1985. Experimental determination of pyroxene compositions in the system CaO-MgO-$Al_2O_3$-$SiO_2$ at 900–1200 °C and 10-15 kbar using PbO and $H_2O$ fiuxes. J. Am. Mineral. 70, 678–695.

Taghizadeh-Farahmand, F., Afsari, N., Sodoudi, F., 2014. Crustal thickness of Iran from converted waves. J. Pure. Appl. Geophys. 172, 309–331.

Tsuchiyama, A., 1985. Dissolution kinetics of plagioclase in the melt of the system diopside-albite-anorthite, and origin of dusty plagioclase in andesites. J. Contrib. Mineral. Petrol. 89, 1–16.

Vernon, R.H., 2008. A Practical Guide to Rock Microstructure. Cambridge University Press, pp. 579.

Vyhnal, C.R., Mcsween, H.Y., Speer, J.A., 1991. Hornblende chemistry in southern Appalachian granitoids: implications for aluminum hornblende thermo barometry and magmatic epidote stability. J. Am. Mineral. 76, 176–188.

Wallace, G.S., Bergantz, G.W., 2002. Wavelet-based correlation (WBC) of zoned crystal populations and magma mixing. J. Earth. Planet. Sci. Lett. 202, 133–145.

Whitney, D.L., Evans, B.W., 2010. Abbreviations for names of rock-forming minerals. J. Am. Mineral. 95, 185–187.

Yousefi, F., Sadeghian, M., Samyari, S., Ghasemi, H., 2016. Geochemistry and tectonic setting of high silica adakitic domes of Ahmad Abad Khartouran (South East of Shahrood). J. Scientific Quarterly Journal, Geosciences 100, 291–298 (In Persian).

Yousefi, F., Sadeghian, M., Wanhainen, Ch., Ghasemi, H., Frei, D., 2017. Geochemistry, petrogenesis and tectonic setting of middle Eocene hypabyssal rocks of the Torud–Ahmad Abad magmatic belt: An implication for evolution of the northern branch of Neo-Tethys Ocean in Iran. J. Geochem. Explor. 178, 1–15.